Astron. Astrophys. 325, 1001–1012 (1997)

ASTRONOMY
AND
ASTROPHYSICS

The X-ray view of the central part of IC 1396

N.S. Schulz[1,2], **T.W. Berghöfer**[2], **and H. Zinnecker**[3]

[1] Massachusetts Institute of Technology, Cambridge MA 02139, USA
[2] Max-Planck-Institut für extraterrestrische Physik, D-85740 Garching bei München, Germany
[3] Astrophysikalisches Institut Potsdam, An der Sternwarte 16, D-14482 Potsdam, Germany

Received 9 August 1996 / Accepted 14 January 1997

Abstract. The galactic HII region IC 1396 contains one of the youngest known open star clusters Trumpler 37, Tr 37. Its very core hosts the multiple O-star system HD 206267, which in many respects is similar to the Orion Trapezium. So far X-ray emission has been observed only from HD 206267 with the *Einstein* observatory. Soft X-ray observations with the *ROSAT* PSPC revealed X-ray emission from an area of 30' radius around the center of globule IC 1396A, which was resolved into 85 discrete sources. Some of the emission still remains unresolved. Most of the detected X-ray sources, except HD 206267, are very weak, which causes the measured luminosity function to be cut off at log $L_x < 30.3$(erg s^{-1}). X-ray sources are located not only in Tr 37 but are also scattered around the molecular globule IC 1396A. From the distribution of sources, their apparently hard spectra, and a steep luminosity function we argue that this sample contains a large number of previously unknown low-mass PMS stars. The X-ray source centered on HD 206267 appeared extended indicating a multiple source system at the very center of Tr 37. The total X-ray luminosity of the trapezium HD 206267 does compare with the X-ray luminosity of single O-type stars. We set an upper limit of log(L_x/L_{bol}) to -6.90 and briefly discuss this result in the context of colliding and eclipsing wind models in early type binaries.

Key words: X-rays: stars – stars: formation – stars: early-type – stars: pre-main sequence

1. Introduction

IC 1396 is an extended HII region at a distance of about 800 pc (Simonson 1968). Its position is near the galactic plane at l = 99.3° and b = 3.74°. This location coincides with the core of the Cep OB2 association. Cep OB2 is divided in two subgroups which differ in age: 1) An older and more dispersed group of roughly 75 O- and B-stars (Simonson 1968) confined within a maximum size of 170 pc (Garmany & Stencel 1992) with an estimated age of 6-7 million years; 2) The young open star cluster Trumpler 37 with an age of 3 million years (Simonson 1968) in its core. The nucleus of the cluster bears the Trapezium-like star complex HD 206267. Its hottest component, an O6.5f star (Walborn & Panek 1984), is the main source of excitation of IC 1396. A proper motion study Marshall & van Altena (1987) identified over 480 stars with a probable membership of $> 80\%$ towards Trumpler 37 within a radius of ~ 7 pc from HD 206267.

The vicinity of IC 1396 has also been identified as a T association. Kun (1986) and Kun & Pasztor (1990) reported of over 200 faint Hα emission line stars being members of Cep OB2. These stars are probably of F-G type with masses below 3 $M_\odot$ in their pre-main sequence stage. An analysis of the color-magnitude diagram of the brightest members of Trumpler 37 as well as several members of Kun's study in the vicinity of HD 206267 indicated that low mass pre-main sequence (PMS) stars should also exist in Trumpler 37 itself (Marshall et al. 1990).

IC 1396 is quite rich in bright rimmed globules. Such globules are usually found in presumably old H II regions and resemble relatively compact and massive areas of H II interacting with the surrounding neutral and cooler gas. In particular the bright rimmed clouds IC 1396 A and B (Pottasch 1956), which are centered $\sim 30'$ to the west of HD 206267, have been the focus of previous investigations in the infrared, sub-millimeter and radio domain (Matthews 1979, de Muizon et al. 1980, Wootten et al. 1983, Nakano et al. 1989). Near the center of IC 1396 A two very young T-Tauri stars ($\sim 10^5 yr$) have been identified, LkHα349 and LkHα349/c being 17 arcsec apart (Herbig & Rao 1972, Cohen & Kuhi 1979)). The latter authors found that both stars may have been born simultaneously and are still in the pre-main sequence stage. The spectral types were given as F8 for LkHα349 and K7 for LkHα349/c with bolometric luminosities of 84 $L_\odot$ and 9$L_\odot$ respectively. From measurements of the CO structure Nakano et al. (1989) suggested that the central part of this globule resembles a cavity that is formed by an interaction of the stellar wind from the central PMS stars and the globule.

The *Einstein* observatory observed a variety of 'classical' star forming regions, e.g. the Taurus-Auriga complex (Gahm 1980, Feigelson & deCampli 1981, Walter & Kuhi 1981, 1984) or the Orion Nebula (Ku et al. 1982, Pravdo & Marshall 1981),

Send offprint requests to: N.S. Schulz, nss@space.mit.edu

and could identify a large fraction of T Tauri stars in X-rays at a level that was $10^3 - 10^4$ times that of ordinary main sequence stars. Geier et al. (1995) investigated a ROSAT PSPC observation of the Orion Nebula region and found 171 X-ray sources in a 20 arcmin radius of the Trapezium with X-ray luminosities above 3.5×10^{29} erg s^{-1} . Most of these sources were identified with PMS stars, 51 of them show spectral types later than F0. Similar to the findings of Freyberg & Schmitt (1995), who investigated stellar clusters in NGC 2023 and NGC 2024 with *ROSAT* , these sources all showed hard ($\sim$ 1 keV) spectra and luminosities up to 10^{31} erg s^{-1} . A more detailed picture of the X-ray emission from the region around the Orion Trapezium is presented by Gagné et al. (1995). Based on three deep ROSAT HRI observations of the Orion Nebula they found 389 X-ray sources, about two-thirds are late-type PMS associated with the cluster. Recent studies of the Taurus region with the the *ROSAT* All-Sky Survey (Neuhäuser et al. 1994) could further confirm that most of the X-ray emitters do not only have hard spectra and high luminosities, but also mostly weak H α emission lines in the optical spectrum. The investigation of the Taurus-Auriga complex with *Einstein* had already hinted that young objects identified in the optical domain with weak H α emission are preferred X-ray emitters compared to classical T Tauri stars with strong H α lines (Walter et al. 1988).

The trapezium system HD 206267 consists of a very luminous (V=5.6) main component of type O6.5V and three fainter stars, component B at 1".6 (V=13.6), component C at 11".7 (B1V, V=8.1) and component D at 19".9 (B2IV, V=8.0) angular distance. The main component itself has long been classified as a spectroscopic binary with an orbital period of 3.7 days (Plaskett 1923). From a recent analysis of IUE spectra, Stickland (1995) concluded the existence of an additional third eclipsing O star component. For the two brightest components, A_1 and A_3, Stickland estimated spectral types O5V and O7/8V with a total mass of 40 $M_\odot$. Recently an additional speckle component (CHARA 212 Aa) to HD 206267A was identified at a distance of roughly 0".1 (Mason 1995).

Einstein observations revealed the O star system HD 206267 and a small number of B stars as sources of soft X-ray emission in IC 1396. Chlebowsky et al. (1989) reported an X-ray luminosity of log L_x = 32.7 erg s^{-1} for HD 206267; the B stars listed in Grillo et al. 1992 typically show X-ray luminosities of log $L_x < 31.5$ erg s^{-1} .

The paper presented here is structured as follows: First, in Sect. 2 and 3 we present the ROSAT observations of IC 1396 and describe our methods of source detection and identification. Second, we take a detailed look at the results for the multiple O star system HD 206267 (Sect. 4), the globules IC 1396 A and B (Sect. 5), and the stellar X-ray emitters in IC 1396 (Sect. 6). Finally, in Sect. 7 we summarize and conclude on our findings.

2. Observations with *ROSAT*

The observations were carried out with the *ROSAT* observatory (Trümper et al. 1983), which was launched in 1990. During its first year in orbit *ROSAT* performed an all-sky survey (RASS) with the position sensitive proportional counter (PSPC, for details see Pfeffermann et al. 1986). During the RASS the Cep OB2 field was observed during two time periods, in August 1990 and January 1991. With a field of view of the PSPC of roughly 2° diameter, each source remains within the field of view up to a time of $\sim$ 30s at the on-axis position during each scan. However, the total exposure in the RASS varies with ecliptic latitude, therefore the exposure times towards the Cep OB2 field vary between 525 s and 1125 s.

Two pointings with the PSPC towards the center of IC 1396 were performed. The first pointed observation, which we will refer to as 'pointing 1' from here on, was carried out between the 26th and the 27th of January 1993 with a net observing time of 8.2 ksec. It was divided into three time windows which lasted 2959 s, 2448 s, and 2796 s spread over a total time interval of 25 hours. The pointing direction was α(2000)=$21^h37^m59^s.0$ and δ(2000)=56°49'48", which is $\sim$ 45 arcmin off-axis to the center of the nebula. The second pointing, which we will refer to as 'pointing 2', was carried out 5 month later on the 21st of June 1993 towards α(2000)=$21^h36^m50^s.4$ and δ(2000)=57°31'12". This is only a few arc minutes off-axis from HD 206267. Pointing 2 lasted for 11.6 hours containing also three observation windows of 1925 s, 990 s, and 1540 s respectively, which gives a net observing time of 4.4 ksec.

The PSPC point spread function is strongly dependent on the off-axis angle: at high off-axis angles the structure of the point spread function gets increasingly complicated as well as extended up to 2 arc minutes. For source detection and identification only pointing 2 is suitable because of its good ($\sim$ 30 arcsec) resolution at the center of the PSPC, which also coincides with the area of interest containing HD 206267, IC 1396A, and IC 1396B. In pointing 1 the center of IC 1396 is highly off-axis and most emission from the center of the nebula appears diffuse and does not allow us to resolve all single sources. It can be used for spectral and time variation analysis, which was especially applicable to the analysis of X-rays from HD 206267.

All data reduction was performed with the X-ray analysis software package EXSAS (Zimmermann et al. 1993). The deduced count rates were corrected for vignetting of the telescope as well as losses caused by deadtime.

3. Source detection and identifications

Source detection has been performed on the RASS observation as well as on pointing 2 using the same detection algorithm. The X-ray analysis software package EXSAS offers a variety of detection methods, which are all based on a maximum likelihood technique (Cruddace et al. 1988). On both fields we applied a local as well as a map source detection. However, source detection and background determination in the survey field was done in one energy band (0.1 - 2.4 keV) only, while in the pointed observation we applied it to five different energy bands (band A = 0.1 - 0.4 keV, band B = 0.5 - 2.0 keV, band C = 0.5 - 0.9 keV, band D = 0.9 - 2.0 keV, and 0.1 - 2.4 keV). Local and map source detections were merged in each field and source positions again tested with the maximum likelihood technique. The detection

Table 1. Source list from survey and identifications

#	α_{2000}	δ_{2000}	cts/s	source ident.	type
1	$21^h31^m01^s.7$	59°25′08”	0.245	HD 205113	K0
2	$21^h49^m17^s.1$	59°23′04”	0.054		
3	$21^h42^m37^s.9$	58°51′17”	0.015	HD 239741	F5
4	$21^h38^m45^s.9$	58°35′49”	0.035		
5	$21^h47^m35^s.2$	58°16′47”	0.073	HD 207514	G0
6	$21^h37^m28^s.4$	57°48′14”	0.016		
7	$21^h42^m23^s.4$	57°44′13”	0.012	HD 206773	B0
8	$21^h22^m19^s.6$	57°34′02”	0.166	HD 203802	G5
9	$21^h40^m22^s.1$	57°34′57”	0.263	HD 206482	F5
10	$21^h38^m56^s.8$	57°29′21”	0.086	HD 206267	O6
11	$21^h23^m11^s.6$	57°16′54”	0.173		
12	$21^h37^m41^s.4$	56°59′22”	0.017	HD 239718	G0
13	$21^h27^m44^s.9$	56°56′36”	0.305		
14	$21^h34^m34^s.4$	56°32′58”	0.077	HD 239702	G5
15	$21^h26^m05^s.7$	55°50′24”	0.192		
16	$21^h29^m26^s.2$	55°33′17”	0.061		

threshold in the survey was set to 4 σ and in pointing 2 it was set to 5 σ. In the latter case we also tried to recover very faint sources and allowed a detection limit of 3 σ. These cases are especially marked if referred to.

3.1. The RASS X-ray field

During the survey mode, sensitivity and spatial resolution are limited due to relatively small exposure times (∼1.5 ksec) and the degrading detector point spread function of the PSPC towards higher off-axis angles. Therefore source detection was performed on a field which was binned to a pixel size of roughly 1.5 arcmin. The bottom part of Fig. 1 shows the IC 1396 field as observed during the RASS. The field appears rather empty with only a few sources in the center and towards the lower right half of the field. We detected 16 sources which could mainly be identified with the *SIMBAD* catalog as main sequence stars. All derived fluxes exceeded 3.7×10^{-13} erg cm^{-2} s^{-1} . A source list together with the *SIMBAD* identifications is given in Table 1. The source numbers correspond to the numbers indicated in Fig. 1. There are a few sources which were not identified. With the exception of the two faint sources #4 and #6 all these sources appear outside the projected area of the nebula. This may hint that those sources are background sources which were not absorbed by the hydrogen clouds of the nebula. On the other hand most identified objects are merely stars in the foreground or within the nebula. HD 206482, for example is a foreground main sequence star of spectral type F0 at a distance of 50 pc, while HD 206773 and HD 206267 have been identified as members of Trumpler 37. At the center of the field, which is mainly occupied by the bright sources HD 206482 and HD 206267 no further X-ray emission was observed in the RASS.

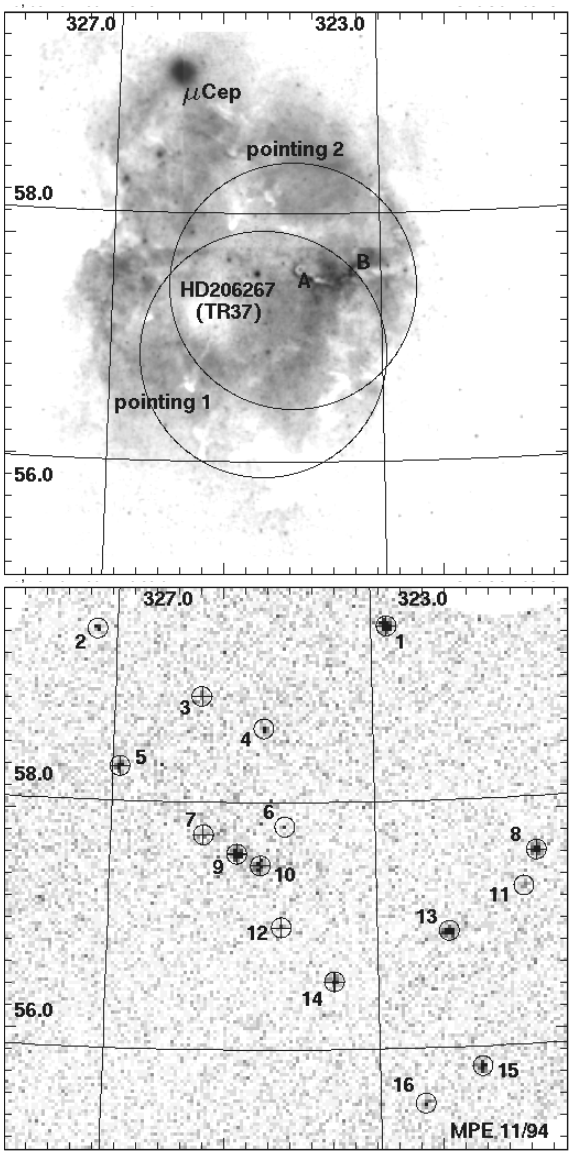

Fig. 1. Top: The extended HII nebula IC 1396 has been scanned from three Palomar Sky Survey Plates. *ROSAT* Pointing 1 covers the center of the nebula only at large off-axis positions; pointing2 observed globule IC 1396A at a nearly on-axis position. **Bottom:** The ROSAT all sky survey (RASS) observation of IC 1396. The field of view is similar to the one of the optical image shown on top. Within this field 16 sources were found above a 4 σ detection level. Source positions and identifications are listed in Table 1 corresponding to the numbers in this figure.

3.2. Pointing 2

The pointed mode offered a much deeper view into the center of the nebula. Sensitivity during one pointing is enhanced due to a much better spatial resolution of ∼ 30 arcsec at the center of the PSPC. Also exposure times were a factor of 5 to 10 higher than in the survey mode. This allowed the detection of X-rays fluxes down to the order of 3×10^{-14} erg cm^{-2} s^{-1} . The source detection algorithm found 44 sources within a 30 arcmin radius

around the centers of Tr 37 and the globule IC 1396A with a probability of existence higher than 5 σ. In addition 28 weak sources with at least 3 σ were found. Positions, exposure times, count rates and X-ray fluxes between 0.1 and 2.0 keV are listed in Table 2, columns 2, 3, 4, and 7 respectively. The source density within 5 armin of the center of emission is 270 sources per square degree. Assuming column densities between 3×10^{21} cm^{-2} at HD 206267 (Chlebowski et al. 1989) and 1.5×10^{22} cm^{-2} at the outer rim of IC 1396A (Nakano et al. 1989) fluxes in the range 0.1 and 2.0 keV vary between 4 - 6 $\times 10^{-14}$ erg cm^{-2} s^{-1} for most of the weak sources and 3 $\times 10^{-12}$ erg cm^{-2} s^{-1} for the brightest source HD 206267 (source #69 in Table 2). The F0-type foreground star HD 206482 (see RASS) was excluded from the sample. A significant portion of unresolved flux remained with a flux level above 1×10^{-13} erg cm^{-2} s^{-1} . Assuming a spectrum from a thermal plasma as derived from Raymond & Smith (1977) with a temperature level of 1.0 keV and absorption column densities in the range mentioned above, we obtain luminosities for these sources between log $L_x \sim 30.5$ and 31.5 for a distance of 0.8 kpc. This range of luminosities is quite typical for young low-mass as well as early type stars.

For most of the detected X-ray sources the number of collected counts is too low for a detailed analysis of the X-ray spectrum. In order to investigate the spectral properties of the X-ray sources we, therefore, calculated the hardness ratios and compared them to model hardness ratios derived for a range of different plasma temperatures and interstellar absorption column densities. The hardness ratios HR1 and HR2 given in Table 2 (column 5 and 6) are defined as follows:

$$\mathrm{HR1} = \frac{\mathrm{B} - \mathrm{A}}{\mathrm{B} + \mathrm{A}} \qquad \mathrm{HR2} = \frac{\mathrm{D} - \mathrm{C}}{\mathrm{D} + \mathrm{C}} \tag{1}$$

A, B, C, and D denote the source counts detected in the energy bands defined above (cf. Sect. 3). The model hardness ratios were calculated by simulating a hot, optically thin plasma (Raymond & Smith 1977) with interstellar absorption for a grid of X-ray temperatures in the range $k \cdot T_x = 0.05 - 2.4$keV and hydrogen absorption column densities $\log(N_H/cm^2) = 18.0 - 22.0$.

Table 2 also lists possible source identifications with various source catalogs (Column 8). The information given in this column contains, if available, the confirmed membership towards the Cep OB2 association, Trumpler 37 (Tr37), or Hα emission stars. The positions were compared to several different catalogs: 'gsc' are entries from the Hubble Space Telescope Guide Star Catalog (GSC; Lasker et al. 1990), 'MVA' sources are from a photometric study investigating the membership in Trumpler 37 by Marshall et al. 1987, 'KUN' labels Hα emission stars from Kun & Pasztor 1990. For MVA and KUN sources no further spectroscopic information was available. Therefore we added the magnitude of the star instead. Finally the deviation of the X-ray position from the optical position was given in brackets. Only pointing 2 has been used, except for the identification of HD 239725 (see below), for source detection and identification in the central region of IC 1396. Fig. 2 shows a contour line plot in which the lowest contour corresponds to a flux level of $\sim 2.5 \times 10^{-14}$ erg cm^{-2} s^{-1} . Each higher contour then increases by a factor of 2.

3.2.1. X-ray sources from *Einstein*

The *Einstein* catalog of O-type stars (Chlebowski et al. 1989) lists three stars that are members of the Cep OB2 association. However, only HD 206267 was in our field of view. This star complex was clearly identified in the RASS as well as in both pointed observations. The position of the X-ray source in pointing 2 was within 5 arcsec. A detailed description of this source will be given in Sect. 4.

We correlated the observed X-ray emission with an $1^\circ \times 1^\circ$ EINSTEIN IPC field centered on HD 206267. These data did not show source detections other than HD 206267 and HD 206482, the foreground F-star, which was also seen in the RASS. This was also confirmed by the *Einstein* source catalog (Harris et al. 1993). The catalog of B-type stars published by Grillo et al. (1992), however, contains 9 entries within the field of view. We marked them with filled squares in Fig. 2. The identification criteria in the catalog of Grillo et al. were that the X-ray source had to be within a 2 arcmin radius of the position given in the SAO catalog of stars. The fluxes of these sources varied between log f_x(erg cm^{-2} s^{-1}) = -12.0 to -12.7 between 0.16 and 3.5 keV. For only two of them we could confirm the identifications with SAO stars. Two remain as candidates with an offset from the SAO position of more than 1 arcmin. The remaining positions are offset by more than 1.5 arcmin and should not be considered as identifications.

3.2.2. Correlations with catalogs

With the SAO catalog of stars as had been used with *Einstein* and the *SIMBAD* catalog used for RASS identifications we were able to identify the bright stars in the field of view. Most of the members of Tr 37 for example are rather faint with magnitudes above m=15.0. The Hubble Guide Star Catalog turned out to be the richest source for identifications. We found 28 entries of this catalog within the FWHM of the point spread function of an X-ray source (see Table 2). The visual magnitudes of these stars range from 7.8 (#52) to 14.5 (#35, #78). The GSC however does not have any information about the spectral type of the entry. Therefore we also looked into more specialized catalogs.

In a study of a possible membership of stars within a 45' radius of HD 206267, Marshall & van Altena (1987) presented a catalog of positions of 1387 stars. From a proper motion study they concluded that 486 stars have a probable membership of $> 80\%$ towards Tr37. From this sample we found 13 objects within 40" of a detected X-ray source. Visual magnitudes of the correlated MVA stars lie between 14.7 for the faintest and and 10.3 for the brightest one. For most of these sources we stated the projected distance to positions found with the GSC in Table 2. Nevertheless, in order to see how the positions of Tr 37 members relate to the observed X-ray emission region, we plotted 120 of the photometrically brightest members into Fig. 2 using filled triangles (from Marshall et al. 1990). As one can see,

Table 2. Source list from pointed observations and identifications (see Sect. 3.2)

#	$\alpha, \delta(2000)$	Exp. (sec)	cts/s 10^{-3}	HR1	HR2	L_x $10^{30} erg \cdot s^{-1}$	identification
1	$21^h31^m12^s.3$ +57°30′28”	2953	10.2 ± 2.5^b	≥0.69	≤0.12	22.1 ± 5.4	
2	$21^h33^m52^s.6$ +57°20′22”	3641	6.7 ± 1.8	≥0.53	≥0.04	14.6 ± 3.9	gsc3975.1178, V=12.1 (2”)
3	$21^h34^m13^s.0$ +57°26′58”	3128	3.6 ± 1.4	≥0.23	≤-0.02	7.8 ± 3.0	
4	$21^h34^m21^s.0$ +57°30′49”	3052	9.0 ± 2.0	≥0.76	0.62±0.08	19.7 ± 4.2	IRAS 21327+5717C (78”)
5	$21^h34^m38^s.0$ +56°32′23”	5493	49.3 ± 3.4	≥0.91	0.40±0.03	0.09 ± 0.006	HD 239702, G5, V=9.5 (41”)[f]
6	$21^h34^m45^s.2$ +57°01′37”	9207	9.6 ± 1.0	≥0.85	0.19±0.07	20.9 ± 2.1	gsc3975.1692, V=13.9 (13”)
7	$21^h34^m58^s.6$ +57°24′57”	4037	2.0 ± 0.9	≥0.19	–	4.5 ± 1.8	
8	$21^h34^m59^s.1$ +57°18′55”	3269	3.2 ± 1.5^b	≥0.24	≥0.62	6.8 ± 4.5	
9	$21^h35^m02^s.9$ +57°28′29”	4240	3.3 ± 1.0	≥0.52	≥0.15	7.1 ± 2.1	
10	$21^h35^m16^s.1$ +57°33′56”	4256	2.1 ± 1.1^b	≥0.23	–	4.5 ± 2.4	gsc3975.550, V=14.3 (5”)
11	$21^h35^m18^s.5$ +57°26′49”	4181	3.7 ± 1.1	≥0.64	-0.01±0.1	8.1 ± 2.4	IRAS 21338+5711 (75”)
12	$21^h35^m24^s.4$ +57°31′26”	4365	5.4 ± 1.2	≥0.77	0.46±0.10	11.6 ± 2.7	gsc3975.604, V=10.0 (8”)
13	$21^h35^m27^s.4$ +57°16′15”	9477	14.6 ± 1.2	-0.27±0.08	0.07±0.16		[f]
14	$21^h35^m28^s.3$ +57°28′39”	4354	3.0 ± 1.0	≥-0.09	≤-0.18	6.6 ± 2.1	
15	$21^h35^m31^s.8$ +57°31′17”	4291	1.5 ± 0.7	≥0.18	≥0.42	3.3 ± 1.5	
16	$21^h35^m35^s.1$ +57°28′48”	4362	4.3 ± 1.2	≥0.53	≥0.42	9.3 ± 2.7	
17	$21^h35^m46^s.4$ +57°36′38”	4379	5.4 ± 1.2	≥0.84	≥0.85	11.7 ± 2.7	
18	$21^h35^m53^s.6$ +57°16′03”	4035	2.4 ± 1.0^a	–	–	5.4 ± 2.1	
19	$21^h35^m54^s.4$ +57°12′08”	8221	4.3 ± 0.7^b	≥0.52	≤0.08	9.3 ± 1.5	
20	$21^h35^m56^s.5$ +57°05′03”	3732	4.9 ± 1.6^b	≥0.59	≥0.23	10.8 ± 3.6	Tr37 Kun59 V=14.2 (3”)
21	$21^h35^m57^s.3$ +57°20′43”	4308	2.3 ± 0.8^b	≥0.41	≥0.26	5.1 ± 1.8	gsc3975.505, V=10.1 (11”)
22	$21^h36^m02^s.9$ +57°28′10”	4590	2.9 ± 0.9	≥0.11	≤0.13	0.04 ± 0.01	HD 205850, F5, V=8.8 (5.6”)[f]
23	$21^h36^m14^s.7$ +57°18′50”	4302	2.4 ± 1.0	≥-0.28	–	5.1 ± 2.1	
24	$21^h36^m15^s.9$ +57°34′52”	4498	5.6 ± 1.2	≥0.47	0.62±0.09	12.3 ± 2.7	
25	$21^h36^m20^s.1$ +56°48′23”	7256	3.1 ± 0.8	-0.22±0.1	≤-0.26		[f]
26	$21^h36^m23^s.9$ +57°36′32”	4346	1.9 ± 0.8^b	≥0.47	≥0.23	4.2 ± 1.8	
27	$21^h36^m24^s.5$ +57°22′28”	4583	1.7 ± 0.7	≥0.46	≥0.59	3.6 ± 1.5	
28	$21^h36^m37^s.7$ +57°34′12”	4693	2.3 ± 0.8	≥0.00	≥-0.07	4.8 ± 1.8	gsc3975.569, V=11.0 (8”)
29	$21^h36^m40^s.9$ +57°30′07”	4753	2.9 ± 0.9	≥0.45	≥0.57	6.3 ± 2.1	HD 239710, B3V, V=9.0 (2”)
30	$21^h36^m49^s.0$ +57°39′13”	4313	2.4 ± 0.9	≥0.48	≥0.55	5.1 ± 1.8	gsc3975.315, V=10.3 (8”)
31	$21^h36^m51^s.9$ +57°31′06”	4791	2.3 ± 0.8	≥0.13	≥0.61	5.1 ± 1.8	gsc3975.396, V=12.8 (11”)
32	$21^h36^m53^s.9$ +57°27′59”	4511	2.7 ± 0.9	≥0.23	≥0.68	6.0 ± 1.8	
33	$21^h36^m58^s.2$ +56°34′43”	5555	3.0 ± 1.0	≥-0.12	–	6.6 ± 2.1	
34	$21^h36^m58^s.5$ +57°23′23”	4445	3.1 ± 0.9	≥0.46	-0.10±0.1	6.6 ± 2.1	IRAS 21352+5610 (55”)
35	$21^h36^m59^s.5$ +57°42′41”	4208	4.3 ± 1.1	≥0.38	-0.03±0.1	9.3 ± 2.4	gsc3975.60, V=14.5 (7”)
36	$21^h37^m00^s.7$ +57°25′27”	4588	1.8 ± 0.7	≥0.39	≥-0.12	3.9 ± 1.5	
37	$21^h37^m00^s.7$ +57°00′31”	7922	3.9 ± 0.8	0.26±0.11	-0.04±0.1		gsc3975.987, V=12.6 (14”)[f]
38	$21^h37^m06^s.3$ +57°12′15”	9003	7.4 ± 0.9	≥0.77	0.08±0.10	16.2 ± 2.1	gsc3975.918, V=10.2 (5”)
39	$21^h37^m06^s.8$ +57°32′03”	4605	3.3 ± 0.9	≥0.40	≥0.64	7.2 ± 2.1	gsc3975.450, V=13.3 (23”)
40	$21^h37^m10^s.5$ +57°31′11”	4736	5.1 ± 1.1	≥0.69	0.39±0.11	11.1 ± 2.4	
41	$21^h37^m11^s.1$ +57°26′10”	4530	6.4 ± 1.3	≥0.76	0.20±0.10	13.8 ± 2.7	gsc3975.339, V=12.6 (3”)
42	$21^h37^m11^s.2$ +57°30′28”	4734	9.2 ± 1.7	≥0.83	≥-0.17	20.1 ± 3.6	
43	$21^h37^m12^s.3$ +57°33′26”	4456	3.2 ± 1.0	≥0.48	≥0.77	0.03 ± 0.01	HD 239715, G0, V=9.5 (41”)[f]
44	$21^h37^m17^s.0$ +57°28′16”	4602	1.9 ± 0.9^b	≥0.32	≥0.05	4.2 ± 2.1	
45	$21^h37^m20^s.6$ +57°30′59”	4671	1.9 ± 0.8	≥0.64	≥-0.04	4.2 ± 1.5	gsc3975.10, V=11.9 (12”)
46	$21^h37^m23^s.0$ +57°31′35”	4628	3.8 ± 1.2	≥0.77	–	8.4 ± 2.4	Tr37 MVA181, V=11.8 (39”)
47	$21^h37^m28^s.0$ +57°23′30”	4296	2.4 ± 1.2^b	≥0.33	–	5.1 ± 2.4	Tr37 MVA144, V=12.2 (36”)
48	$21^h37^m30^s.9$ +57°48′12”	3052	22.2 ± 2.9	-0.04±0.07	0.18±0.09		[f]
49	$21^h37^m35^s.1$ +56°45′06”	7445	1.4 ± 0.6^a	≤-0.65	–	3.0 ± 1.2	
50	$21^h37^m39^s.3$ +56°55′05”	8186	1.5 ± 0.5	≥0.23	≥0.06	3.3 ± 1.2	gsc3975.1070, V=13.1 (5”)
51	$21^h37^m43^s.0$ +57°36′21”	4192	2.1 ± 1.0^b	≥0.18	≤-0.49	4.5 ± 2.1	gsc3975.32, V=12.7 (10”)
52	$21^h37^m43^s.6$ +57°33′28”	4324	1.9 ± 0.8	≥0.18	≥0.36	4.2 ± 1.8	gsc3975.168, V=7.8 (22”)
53	$21^h37^m44^s.4$ +56°59′07”	11442	21.6 ± 1.4	0.20±0.04	≤-0.23	0.15 ± 0.01	HD 239718, G0, V=9.3 (8”)[f]

Table 2. (continued)

#	α, δ(2000)	Exp. (sec)	PSPC cts/s 10^{-3}	HR1	HR2	L_x 10^{30} ergs/s	identification
54	$21^h37^m46^s.9$ +56°51′40”	8079	1.0 ± 0.5^b	≥0.31	≥0.20	2.1 ± 1.2	
55	$21^h37^m50^s.7$ +56°59′08”	8074	2.6 ± 0.7^a	≤-0.12	–		^{f}
56	$21^h37^m51^s.6$ +57°26′47”	4372	8.5 ± 1.5	≥0.82	0.40±0.08	18.6 ± 3.3	gsc3975.364, V=12.8 (6”)
57	$21^h37^m53^s.9$ +56°54′06”	8021	2.2 ± 0.6	-0.17±0.1	≤-0.32		gsc3975.1179, V=9.9 (18”)^f
58	$21^h37^m58^s.2$ +57°31′16”	4367	2.4 ± 0.9	≥-0.04	–	5.1 ± 1.8	gsc3975.447, V=13.1 (19”)
59	$21^h38^m16^s.1$ +57°22′06”	4190	3.4 ± 1.1	≥0.29	≥0.27	7.5 ± 2.4	gsc3975.438, V=13.2 (26”)
60	$21^h38^m19^s.2$ +56°38′26”	7549	1.6 ± 0.6^a	≤-0.49	–		^{f}
61	$21^h38^m20^s.7$ +56°39′23”	7663	3.6 ± 0.9	≥-0.64	–	7.8 ± 2.1	
62	$21^h38^m23^s.1$ +56°37′19”	7057	1.2 ± 0.6^b	≥0.26	≤-0.17	2.7 ± 1.5	
63	$21^h38^m23^s.4$ +56°53′01”	8375	3.7 ± 0.8	≥0.18	0.44±0.11	8.1 ± 1.5	
64	$21^h38^m25^s.8$ +57°34′00”	4017	15.7 ± 2.1	≥0.89	0.58±0.06	34.2 ± 4.5	
65	$21^h38^m26^s.8$ +56°58′24”	7956	6.0 ± 0.9	≥0.62	-0.05±0.08	13.2 ± 2.1	HD 206183, B9, V=7.1 (5”)
66	$21^h38^m27^s.2$ +57°41′39”	3261	4.9 ± 1.5	≥0.83	0.24±0.11	10.8 ± 3.3	gsc3975.289 V=10.5 (22”)
67	$21^h38^m28^s.4$ +56°57′10”	7731	1.8 ± 0.5	≥0.27	-0.15±0.1	3.9 ± 1.2	gsc3975.1430 V= 13.6 (4”)
68	$21^h38^m30^s.8$ +56°53′33”	8337	1.7 ± 0.5	≥0.17	≥0.66	3.6 ± 1.2	
69	$21^h38^m57^s.3$ +57°29′11”	7799	98.7 ± 3.5	≥0.95	0.00±0.03	230 ± 8	HD 206267, O6.5V, V=5.7 (5”)
70	$21^h39^m04^s.8$ +56°56′50”	7645	2.8 ± 0.7	≥0.65	-0.30±0.1	6.0 ± 1.5	HD 239725, B8, V=8.7 (8”)
71	$21^h39^m05^s.3$ +56°51′29”	7807	2.8 ± 0.7	≥0.17	≥0.79	6.0 ± 1.5	
72	$21^h39^m12^s.6$ +57°23′20”	3254	6.1 ± 1.8	≥0.42	≥0.20	13.5 ± 3.9	gsc3975.114 V=13.6 (16”)
73	$21^h39^m18^s.9$ +57°00′38”	7407	2.0 ± 0.7^a	–	–	4.5 ± 1.5	gsc3975.1648 V=11.8 (24”)
74	$21^h39^m20^s.3$ +57°04′02”	3455	38.5 ± 3.5	≥0.84	≥0.87	84.0 ± 7.5	
75	$21^h39^m30^s.5$ +56°59′07”	2008	22.4 ± 4.7^a	≥0.68	≥-0.20	48.9 ± 10.2	
76	$21^h39^m36^s.2$ +56°51′29”	7454	3.3 ± 0.8	≥0.62	≥0.74	7.2 ± 1.8	
77	$21^h39^m41^s.0$ +57°30′23”	7667	1.3 ± 0.5^a	–	–	2.7 ± 1.2	
78	$21^h39^m45^s.7$ +56°13′33”	2646	6.5 ± 2.3	≥0.52	≥0.26	14.4 ± 5.1	gsc3975.300 V=14.5 (15”)
79	$21^h39^m47^s.6$ +57°05′08”	5146	6.2 ± 1.7^b	≥0.64	≥0.76	13.5 ± 3.9	gsc3971.43 V=13.1 (10”)
80	$21^h39^m53^s.4$ +56°41′44”	6297	4.0 ± 1.1	≥0.40	≥0.41	8.7 ± 2.4	
81	$21^h40^m19^s.4$ +56°51′32”	6223	3.3 ± 0.9	≥0.70	0.23±0.12	7.2 ± 1.8	
82	$21^h40^m22^s.1$ +57°35′06”	5676	4.0 ± 1.1	≥0.74	0.26±0.11	0.008 ± 0.002	HD 206482B, V=7.4 (9”)^f
83	$21^h40^m22^s.8$ +57°34′44”	8555	198 ± 5	0.18±0.02	-0.04±0.02	0.43 ± 0.01	HD 206482, F5V, V=7.1 (10”)^f
84	$21^h41^m15^s.0$ +57°45′52”	2934	7.5 ± 2.5^b	≥0.69	–	16.2 ± 5.4	gsc3975.616, V=13.4 (21”)
85	$21^h42^m19^s.8$ +57°44′41”	2453	13.5 ± 3.0^b	≥0.75	≥0.50	29.4 ± 6.6	HD 206773 B0 V=6.87 (72”)

[a] only broad band (0.1–2.4 keV) detection
[b] only hard band (0.1–2.0 keV) detection
[f] foreground star

those sources distribute radially around the cluster center HD 206267, while most of the X-ray emission concentrates on a bar-like structure covering HD 206267 and the two globules IC 1396 A and B (see below).

Another attempt to identify *ROSAT* sources with stars in IC 1396 was done by a correlation with the H α emission star catalog by Kun & Paszdor (1990). Objects from this catalog were labeled with KUN followed by the entry number given in that star list. Unfortunately for most of the objects in the field of interest no indication of the optical emission line strengths were given. However, more recent medium resolution studies of a selection of 35 stars of this sample concluded that they do show only very weak Hα emission (Balazs et al. 1996). Direct identifications with this catalog were also rather sparse. Only source #20 in Table 2 was within 3” of a 14th magnitude emission star. Another candidate, source #59, was found within 26” of a 13th magnitude emission star, but it coincides with a 15th magnitude star from the MVA list being 6” apart from the emission line star. The emission line star was also found in the GSC. Source #31 appears within 11” of the Herbig star LkHα349. All other objects do not coincide with any detected X-ray source within a search radius of 1’. A variety of emission line stars, however, coincide with unresolved X-ray emission. We plotted all objects of the KUN catalog that lie within the field of view in Fig. 2 with filled diamond symbols.

Kun & Paszdor (1990) also examined over 140 IRAS point sources in or in the vicinity of IC 1396. It became apparent that those objects are not correlated with Tr 37 but are merely projected onto the dark clouds around the HII regions. From this list of IRAS point sources we did not find any candidates suitable for an identification. One object, IRAS 21338+5711, was found within a distance of 75” within source #11. In a search for embedded young stellar objects by Schwartz et al. (1991) there were another two candidates, which are rather close to

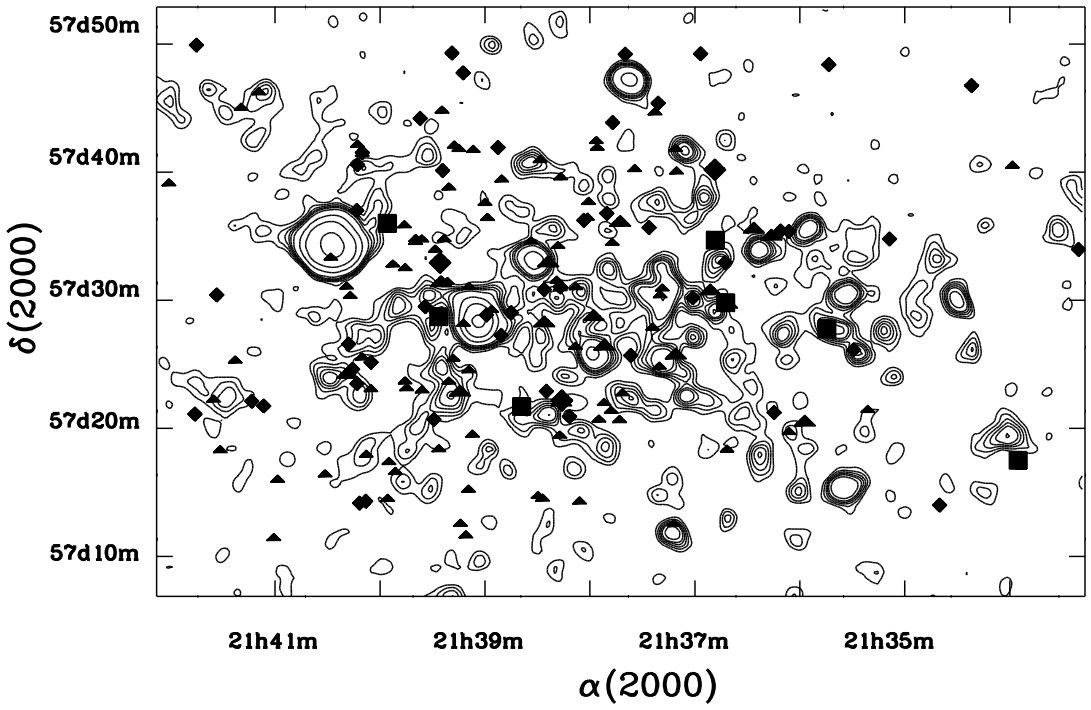

Fig. 2. X-ray contours from the center of IC 1396. The symbols refer to entries in various source catalogs: triangles for members of Trumpler 37 (Marshall et al. 1987), diamonds for low-mass Hα emission type stars (Kun & Pasztor 1990), squares for identified X-ray sources with *Einstein* (Grillo et al. 1992).

detected X-ray sources in the globules IC 1396 A (#31, 35") and IC 1396 B ((#4, 78"). The latter object was observed at a large offset angle in the PSPC, which may explain its large deviation (see Sect. 5)

3.2.3. Variability

The search for time variability in data of such limited statistics is a difficult issue. We decided that the best way to do this is to use a Kolmogorov-Smirnov test (KS-test), i.e. to determine the probability of deviation of received events of a single source against a constant lightcurve.

It turned out that most of the sources in this sample, about 80%, do not show any sign of variability above a 90% threshold and only 20% are or may be variable. There is no spatial preference of variable candidates. Source #9 in Table 2 shows a probability for variability of 100% and is a probably a flaring star. Here we found a significant detection only in one of the three observation windows. In the other two windows no detection was made. This was the only case where we saw such a behaviour. A source detection applied on all three observation windows separately support these findings. Only 10% of the sources showed a difference in detection significance of more than σ.

3.2.4. Hardness ratios

Since it is impossible to compute a statistically meaningful spectrum for all sources, except for HD 206267 (source #69 in Table 2), we determined the standard hardness ratios as described above. Only a small number of sources could be detected in all four energy bands. In all other cases we derived upper or lower limits of the spectral hardness. In Table 2 we marked lower limits with "$\geq$" and upper limits with "$\leq$". In Fig. 3, we plot the hardness ratios in a color-color diagram; upper and lower limits are marked with arrows which indicate whether the actual spectrum is expected to be harder or softer. Fig. 3 also shows parameter tracks based on Raymond-Smith type spectra and computed for different Since the interstellar absorption column density along the line of sight towards IC 1396 exceeds $10^{21}\mathrm{cm}^{-2}$ we do not expect to detect any X-ray source in the soft energy band of ROSAT associated with the nebula. Therefore, we use the soft band detection as an additional discriminator between foreground stars and IC 1396 members. In Fig. 3, the foreground stars are plotted as open circles, X-ray sources that could be identified with OB stars are marked with stars, and other IC 1396 members are marked with diamonds. Fig. 3 also shows parameter tracks computed on the basis of interstellar absorbed Raymond-Smith type spectra. The solid lines show modeled hardness ratios for constant interstellar absorption column densities of $\log(N_H)$ = 19.0, 20.0, 21.0 and X-ray temperatures varying between 0.05 and 2.0 keV, the dotted lines corresponds to constant X-ray temperatures of 0.5, 1.0, 1.5 keV

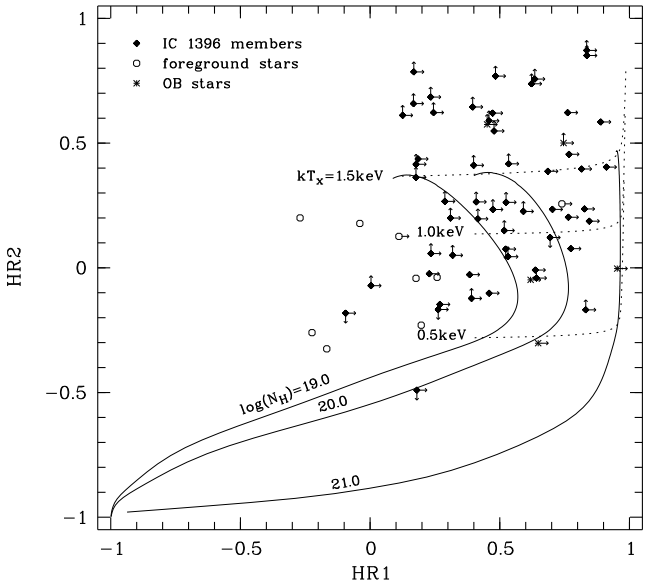

Fig. 3. Hardness ratios HR1 vs. HR2 (as listed in Table 2). In those cases were we could only derive an upper or lower limit for HR1 or HR2 (or both) we indicate the range of possible positions in the plot with arrows. Added are modeled tracks of hardness ratios for standard Raymond-Smith spectra (see text). Different solid lines result from various column densities, while dotted lines correspond to different spectral temperature parameters.

and absorption columns varying between $\log(N_H)$ = 19.0 and 22.0.

As is clear from Fig. 3, most of the IC 1396 members appear to the upper right of the diagram well above the 0.5 keV dotted line, whereas almost all of the foreground stars are located in the center of the plot. The range of the hardness ratios for the IC 1396 members indicate the existence of low-mass pre-main sequence stars with rather hard, i.e near 1 keV spectra (Freyberg & Schmitt 1995). OB-type stars typically show softer X-ray spectra well below 1 keV (Cassinelli et al. 1994, Berghöfer et al. 1996), e.g., the O-star system HD 206267 is located near the 0.5 keV dotted line. Note that the rather hard X-ray spectra of the X-ray sources identified with the B-stars HD 206183, HD 206773, and HD 239710 cast doubt about their association with the X-ray sources. Additionally, since late B stars are not known to produce any X-ray emission, the X-ray emission detected for the late B stars HD 206183 and 239725 is more likely produced by optically fainter low-mass stars. Therefore, the low-mass stars in IC 1396 constitute the bulk portion of the detected X-ray sources.

4. The multiple O star system HD 206267

In all our ROSAT observations, the RASS data as well as both pointed observations, we observed an X-ray source with a count rate of $\approx$ 0.09 – 0.1 cts/s at the optical position of HD 206267. In pointing 2 the source is located within the inner 20 $'$of the detector and the source detection algorithm, which compares the observed point spread function with a theoretical model, provides evidence for an extended source at the $> 8\sigma$ level. A contour plot of the source region shows patches of intensity asymmetrically distributed around the center of the X-ray source. In order to test the influence of the image binning on the source extent we then ran a source detection on an image binned with an artificially higher resolution (a factor of 2 higher than the nominal resolution of the PSPC). The extended X-ray source now splits into five distinct X-ray sources ($> 6\sigma$). Note that we do not claim to have resolved 6 X-ray sources in the vicinity of HD 206267, however, this result suggests the existence of more than a single point source. At any rate, HD206267 is the dominant X-ray source. Note that pointing 1 shows HD206267 at a high off-axis position in the detector and, therefore, does not allow an investigation of the spatial extent of the appropriate X-ray source.

Count rate variations for HD 206267 between the distinct ROSAT observations are low: during RASS and pointing 1 we observe about 0.09 cts/s, pointing 2 shows a slightly higher level (0.1 cts/s) which can be explained by additional sources contaminating the actual X-ray emission of HD 206267 at the large off-axis angle. In order to check for orbit related variations in X-ray count rate we used the ephemeris provided by Stickland (1995) and computed the orbital phases for the times of the ROSAT observations on HD 206267. Unfortunately, all ROSAT observations fall in the range ϕ = 0.27 – 0.54 (primary conjunction is around ϕ = 0.18) and, therefore, our data cannot be used to further investigate orbit related variations in X-ray count rate.

Since the RASS data for HD 206267 consist of only 70 source counts sampled during a total exposure time of $\sim$800 sec, these data cannot be used for a detailed spectral analysis. Therefore, we investigated the X-ray spectral properties of HD 206267 on the basis of our pointed observations. During pointing 1 lasting over about 8 ksec we detected about 700 photons, whereas pointing 2 lasted about half of that time accumulating 360 photons in the X-ray spectrum. In both spectra all emission is observed in the energy range 0.5 – 2.0 keV. We binned the spectra into 19 bins with a signal-to-noise-ratio of at least 4σ and fitted an interstellar absorbed Raymond-Smith type thermal plasma spectrum to the observed spectra. For both observed X-ray spectra we first fixed the interstellar absorption column to the value of $3.07\times10^{21} cm^{-2}$ derived from Lyman α measurements (Shull & van Steenberg 1985). In a second run we treated the interstellar absorption as a free parameter. As is evident from Table 3 which summarizes our fit results for the X-ray spectra of HD 206267, a higher absorption column leads to significantly lower X-ray temperatures which can be explained by intrinsic wind absorption of the X-ray emission of the O star(s). Compared to pointing 1 we obtained for pointing 2 somewhat higher X-ray temperatures. This indicates for pointing 2 a higher source contamination of the O star's X-ray emission by X-ray sources (presumably late-type stars) in the vicinity of HD 206267; late-type stars show temperatures for the X-ray emitting plasma of typically 1.0 keV.

Table 3. Spectral fit parameters for HD 206267

pointing	N_H $\times 10^{21}$ cm^{-2}	kT keV	χ^2/ν
1	3.07(fixed)	0.56±0.13	2.20
	8.59±1.07	0.22±0.04	1.70
2	3.07(fixed)	0.72±0.10	1.66
	8.69±1.03	0.26±0.06	1.99

Assuming a distance of 800 pc and a spectral model with N_H = 3.07 × $10^{21} cm^{-2}$ and T_x = 0.72keV, we derive from the X-ray count rate of 0.09 cts/s an X-ray luminosity of log(L$_x$[erg s^{-1}]) = 32.36. If we consider that the X-ray emission observed at the position of HD 206267 represents the integrated emission of at least 4 early-type stars and additional X-ray emitters that remain unresolved by the ROSAT PSPC observations, the corresponding log(L_x/L_{Bol}) = -6.90 represents an upper limit for the X-ray emission of the hot stars in HD 206267. Note that this value is in accordance with the results of Berghöfer et al. (1996) who studied the X-ray properties of all optically bright OB stars detected in the RASS. For O stars the authors found a mean log(L_x/L_{Bol}) = -6.90 ± 0.36. Compared to the X-ray luminosity of log(L$_x$[erg s^{-1}]) = 32.7±0.31 that Chlebowski et al. (1989) derived for HD 206267 from the *Einstein* observations, we derive from the ROSAT observations a factor of 2.2 smaller X-ray. A comparison of the model-independent X-ray count rates shows a ratio between ROSAT PSPC and *Einstein* IPC count rates of ≈ 2:1. This is a reasonable value for the X-ray spectral properties of HD 206267 and the energy dependent ratio of the effective areas of both detectors which is also a strong argument against the possibility that intrinsic variability is responsible for the discrepancy in X-ray luminosities. It can only be explained by a difference in the energy conversion of the *Einstein* and *ROSAT* count rate. Since we assumed the same spectral model and the same input parameters (N_H, T_x, distance) as Chlebowski et al. , we carefully checked the way we derived the energy conversion factor for the ROSAT data. However, we didn't find any reason to question our result. Therefore, we think the X-ray luminosity given by Chlebowski et al. 1989 overestimates the actual value for HD 206267 by a factor of 2.

5. The globules IC 1396 A and B

Central in the field of view of pointing 2 is the cometary nebula IC 1396A. Its central star LkHα349 is a very young Herbig Ae/Be star (Hessman et al. 1995 and references therein). Within a ∼ 30" radius of LkHα349 two other young faint objects are in the line of sight, LkHα349/c and an IRAS point source (Schwartz et al. 1991). The latter may indicate the existence of a young embedded B-star. The projected position of source #31 in Table 2 is merely in between these objects, but appears closer to LkHα349. However, even with the good resolution of 30" of the PSPC, it may be be problematic to distinguish whether it is significantly separated from the position of the IRAS point source. The X-ray source is detected at more than 5σ with an estimated source flux of log f$_x$ = -12.7. This corresponds to a luminosity of 1.0×10^{30} erg s^{-1} adopting a distance of 750 pc. Clearly this is a conservative value, since in Table 2 we assumed a 0.5 keV spectrum with a log N$_H$ of 21.5, which is below the estimate for the average column density of 22.2 for the globule by Nakano et al. (1989).

Fig. 4 shows the X-ray contours overlayed on an optical photograph containing the two globules. IC 1396A and its vicinity show many distinct point sources with hard spectra (see Schulz 1996) and luminosities comparable to the one observed from LkHα349. IC 1396B, located to the very right in Fig. 4, lacks prominent X-ray emission. This may partly be due to a rather unfortunate obscuration pattern caused by the PSPC window grid structure (Pfeffermann et al. 1986). The only significant point source (#4 in Table 2) at its eastern rim lies close to the IRAS point source 21327+5717C which may be a candidate embedded young stellar object (Schwartz et al. 1991).

6. Stellar X-ray emitters in IC 1396

We used the ROSAT PSPC to investigate the X-ray sources in IC 1396 which is known to be one of the youngest star formation regions in our galaxy. The sensitivity limit of our ROSAT observations constrains the detection of X-ray sources in IC 1396 to an X-ray flux of 3 × 10^{-14} erg cm^{-2} s^{-1} which corresponds to an X-ray luminosity of 2 × 10^{30} erg s^{-1} at a distance of 800 pc. In the following we discuss our findings for the late-type stars and early-type stars in IC 1396 separately.

6.1. Late-type stars

Due to its larger distance compared to other star formation regions like the Orion Nebula or the Chamaeleon star formation region, for example, IC 1396 was rather difficult to study in X-rays. While in these former regions the sensitivity of *Einstein* observations and the RASS proved to be sufficient to detect a large number of previously unknown PMS stars (Feigelson 1987, Gagné & Caillault 1994, Neuhäuser et al. 1995, Alcala et al. 1995), X-rays from young stars in the center of IC 1396 were hardly detectable except for its central star system HD 206267. All the bright sources detected with the RASS could be identified with either foreground stars or members of the Cep OB2 association. In both of our pointed observations with the *ROSAT* PSPC, however, X-rays from an area of 20 arcmin radius around the center of the nebula became clearly evident. Spatial resolution in one of the pointed observations did not allow us to resolve the emission into point sources but it clearly showed the existence of an extended field of X-ray emission. A second observation that pointed directly towards the center of the nebula resolved the emission into 85 point sources and some patches of still unresolved flux. Most of the sources are faint with X-ray fluxes below 6×10^{-13} erg cm^{-2} s^{-1} , however they were detected with a significance higher than 5σ. The direction of the

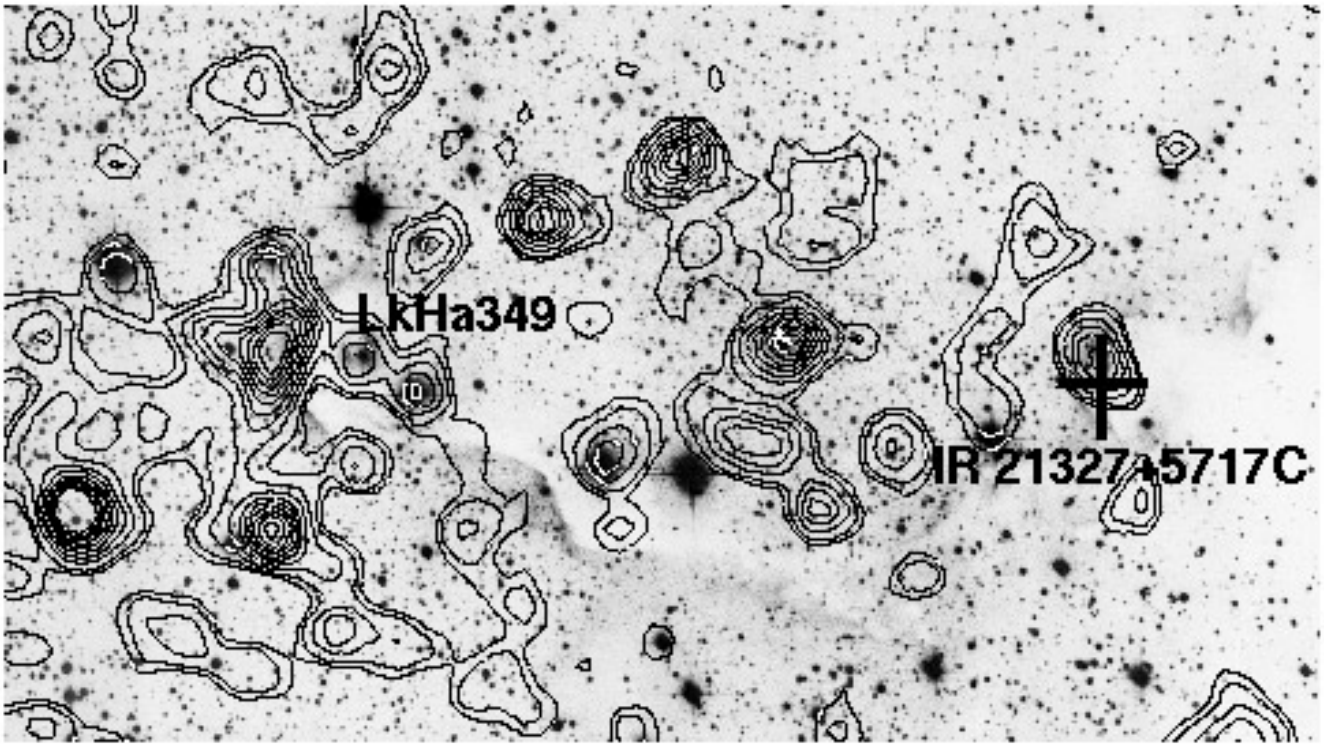

Fig. 4. A 35 arcmin wide view of IC 1396A and B (1 cm corresponds to about 2 arcmin) with overlaid X-ray contours. The cometary globule IC 1396A is to the center left, IC 1396B to the far right with respect to the image center. LkHα349 (source #31 in Table 2) is at the center of globule A.

field of view towards the center of the nebula may lead to the conclusion that we see X-ray emission from young B-stars of Tr 37. Surveys with the *Einstein* Observatory have shown that presumably early-type, i.e. less than B3, stars emit a considerable portion of their bolometric luminosity in X-rays (Long & White 1980). Recently it also has been argued from findings of the RASS that even late type B-stars may be intrinsic X-ray emitters (Berghöfer & Schmitt 1994). In the case of Tr 37, however, the correlation with over 480 photometrically identified members of the cluster revealed that only 15 sources detected in X-rays could be associated with cluster members and only 6 of them were clearly identified. Also the spatial distribution of the cluster members around HD206267 appears to be radial, whereas the bulk of X-ray emission is concentrated in a band that spreads from somewhat east of HD206267 to globules A and B in the west (see Fig. 2).

From the objective prism survey by Kun (1986) and Kun & Pasztor (1990) it became clear that IC 1396 is also a breeding ground for low-mass PMS stars. Although only a small fraction of the emission line stars of the survey were in the actual X-ray field of view, the fact that we could only identify 2 of these objects with X-ray point sources needs explanation. Here the anomalous extinction properties of Tr 37 (Clayton & Fitzpatrick 1987, Roth 1988, Marshall et al. 1990) and the closeness of this area to a group of denser HI clouds (Wendker & Baars 1980) plays a key role. The visual magnitude distribution of the KUN survey peaked around m=14.5. Such a magnitude would correspond to low-mass PMS ($< 3\ M_{\odot}$) at a distance around 800 pc with a foreground extinction of 1.5 mag. Incorporating visual extinction by dust in the nebula itself, the magnitude drops below values of 15 to 16, which is beyond the sensitivity of the Kun survey. Vice versa, E(B-V) variations between 0.42 and 1.10 as observed by Garrison & Kormendy (1976) for bright Tr 37 members imply intrinsic column densities of $\sim 3.6 \times 10^{21} cm^{-2}$ for the nebula, which is about the same as measured in the line of sight towards the nebula. Thus in X-rays as well as in the optical we may only see the tip of the iceberg of the number of low-mass PMS stars within the nebula due to the limited sensitivity of observations.

This view is also supported by the luminosity function. The mean of all X-ray luminosities is log L_x = 30.8 (erg s^{-1}) with a spread of about $\pm$.5, which indicates a rather steep function. From the previous arguments it is conceivable that we do not observe luminosities much below log L_x = 30.3, because of insufficient sensitivity. In Fig. 5 we show the X-ray luminosity function for all (non early-type) member stars of IC 1396 detected in both pointed observations. As can be seen from Fig. 5, the cumulative X-ray luminosity function does compare with the appropriated X-ray luminosity function observed for late-type pre-main sequence stars in the Orion Nebula (cf. Gagné et al. 1995) which demonstrates the similarity of the late-type

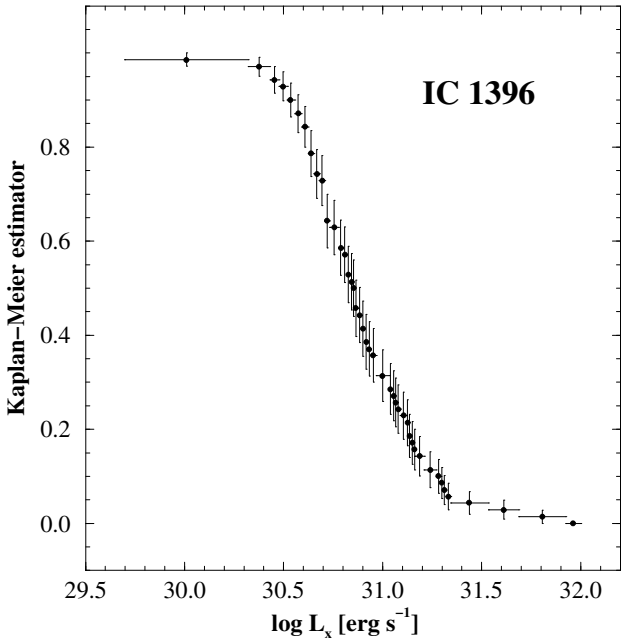

Fig. 5. Cumulative X-ray luminosity function for non-early type members of IC 1396

star content in the Orion nebula region and the IC 1396 region discussed here.

6.2. Early-type stars

Concerning the early-type stars in IC 1396, i.e. Tr 37, we identified only a small number of X-ray sources with early-type stars. The high interstellar absorption column density towards IC 1396 is expected to absorb the mainly very soft X-ray emission of the early-type stars.

HD 206267 is without doubt the brightest X-ray source in the entire sample. Compared to single O stars the multiple O star system HD 206267 seems to show typical X-ray properties. Note that the X-ray emission of HD 206267 could not be separated from the X-ray emission of a small number of weaker X-ray sources in the vicinity of HD 206267 and, therefore, the derived X-ray luminosity of log L_x = 32.36 represents an upper limit for the X-ray output of all O stars bound in HD 206267. In the case of single hot stars the X-ray emission is thought to originate from X-ray emitting shocks in stellar winds. In addition to the X-ray emission generated in the winds of the individual stars, a possible collision of the stellar winds offers a second X-ray emitting mechanism for massive binaries (Cherepashchuk 1976). However, the observed X-ray luminosity of HD 206267 does not provide any evidence for an excess in X-ray emission as predicted by the interacting wind model. The ratio between X-ray luminosity and bolometric luminosity of log (L_x/L_{bol}) = -6.90 is in accordance to the mean value for O-type stars found by Berghöfer et al. (1996). Since the ROSAT observations of HD 206267 fall in a small range of orbital phases of the main binary system in HD 206267, we cannot use our data to study orbit related variability in X-ray count rate. In the case of 29 CMa, Berghöfer & Schmitt (1995) found sinusoidal variations in X-ray count rate by a factor of 2 with a maximum count rate around primary minimum. The authors attribute these variations to a phase-dependent absorption column towards the X-ray emitting regions in both eclipsing stellar winds.

7. Conclusion

We have observed X-rays from the center of IC 1396. Only HD 206267 had already been known as a soft X-ray emitter from *Einstein* observations. Within a field of roughly 40' arcmin radius we also detected 85 X-ray sources of which 13 sources were identified as foreground objects. Since most of the early-type members of the young open cluster Tr 37 should be absorbed, we are very confident that we have observed the X-ray emission of young late-type PMS stars. Their X-ray spectra appear hard with luminosities between log L_x = 30 and 31. The luminosity function compares well to the ones observed from other star forming regions like the Orion nebula. Many of the hard X-ray sources scatter around the molecular globules IC 1396 A and B. LkHα349, a 10^5 yr old T-Tauri star at the very center of globule A, appears very luminous with $L_x = 5.1 \times 10^{30}$ erg s^{-1} .

The trapezium system HD 206267, although the brightest X-ray source of the sample, appears rather faint compared to luminosities of other O-type stars. The X-ray point spread function is clearly extended indicating a multiple X-ray source complex. Thus HD 206267 cannot be considered as a candidate for X-ray generation through colliding winds.

Acknowledgements. We thank Tom Ray, Dan Dewey and J.H.M.M. Schmitt for carefully reading the manuscript. The ROSAT Mission is supported by the Bundesministerium für Forschung und Technologie (BMFT) and the Max Planck-Gesellschaft (MPG). We thank the SASS and EXSAS teams at the MPE for their support. N.S.Schulz's research at M.I.T. is supported in part by the AXAF Science Center as part of Smithsonian Astrophysical Observatory contract SVI–61010 under NASA Marshall Space Flight Center.

References

Alcala J., Krautter J., Schmitt J.H.M.M., et al., A&AS 114, 109
Balazs L.G., Garibjanyan A.T., 1996, A&A 311, 145
Berghöfer T.W., Schmitt J.H.M.M., 1994, A&A, 292, L5
Berghöfer T.W., Schmitt J.H.M.M., 1995, The ROSAT view of the massive eclipsing O-type binary system 29 UW Canis Majoris, In: Hucht, K.v.d., Williams, P.M. (Eds.) Wolf-Rayet Stars: Binaries, Colliding Winds, Evolution, Kluwer Publishers, Dortrecht, p. 382
Berghöfer T.W., Schmitt J.H.M.M., Cassinelli J.P., 1996, A&AS, 118, 481
Berghöfer, T.W., Schmitt, J.H.M.M., Danner, R., Cassinelli, J.P. 1996, A&A in press
Cassinelli J.P., Cohen D.H., MacFarlane J.J., Sanders W.T., Welsh, B.Y.,1994, ApJ 421, 705
Cherepashchuk A.M., 1976, Pis'ma Astron. Zh. 2, 356
Chlebowski T., Harnden F.R., Sciortino S., 1989, ApJ 341, 427
Clayton G.C., Fitzpatrick E.L., 1987, AJ 93, 157
Cohen M., Kuhi L.V., 1979, ApJS 41, 743

Crampton D., Redman R.O., 1975, AJ 80, 454
Cruddace, R.G., Hasinger G.R., Schmitt J.H.M.M., 1988, The Application of a maximum likelihood analysis to detection of sources in the ROSAT data, in: Astronomy from large databases, ed. Murtagh F., Heck A., ESO Conference and Workshop Proc. 28, Garching, 177
de Muizon M., Rouan D., Lena P., et al., 1980, A&A 83, 140
Duvert G., Cernicharo J., Bachiller R., et al., 1990, A&A 233, 190
Feigelsen E.D., DeCampli W.M., 1981, ApJ 243, L89
Freyberg M.J., Schmitt J.H.M.M., 1995, A&A 296, L21
Gagné M., Caillault J.-P., 1994, ApJ, 437, 361
Gagné M., Caillault J.-P., Stauffer J.R., 1995, ApJ, 445, 280
Gahm G.F., 1980, ApJ 242, L163
Garrison R.F., Kormendy J., 1976, PASP, 88, 865
Garmany C.D., Stencel R.E., 1992, A&AS 94, 211
Geier S., Wendker H.J., Wisotzki L., 1995, A&A 299, 39
Grillo F., Sciortino S., Micela G., et al., 1992, ApJS 81, 795
Harris et al., 1993, The Einstein Observatory catalog of IPC X-ray sources. Volume 7E
Herbig G.H., Rao N.K., 1972, ApJ 174, 401
Ku W. H.-M., Righini-Cohen G., Simon M., 1982, Sci 215, 61
Kun M., 1986, Ap&SS 125, 13
Kun M., Pasztor L., 1990, Ap&SS 174, 13
Marschall L.A., van Altena W.F., 1987, ApJ 94, 71
Marschall L.A., Comins N.F., Karshner G.B., 1990, AJ 99, 1536
Mason B.D., 1995, priv. com.
Matthews, H.E. 1979, A&A 75, 345
Nakano M., Tomita Y., Ohtani H., et al., 1989, PASP 41, 1073
Neuhäuser R., Sterzik M., Schmitt J.H.M.M., et al. 1995, A&A 297, 391
Pfeffermann E., Briel U.G., Hippmann H., et al., 1986, Proc. SPIE 733, 519
Plaskett J.S., 1923, PDAO 2, 269
Pottasch, S. 1956, Bull. Astron. Netherlands 13, 77
Pravdo, S.H., Marshall, F.E., 1981, ApJ 248, 591
Raymond J.C., Smith B.W., 1977, ApJS 35, 419
Roth M., 1988, MNRAS 233, 773
Schulz N., 1996, in *Röntgenstrahlung from the Universe*, eds: H.U. Zimmermann, J. Truemper and H. Yorke, MPE report 263, ISSN 0178-0719, 67
Schwartz R.D., Gyulbudaghian A.L., Wilking B.A., 1991, ApJ 370, 263
Simonson III, S.C., 1968, ApJ 154, 923
Shull J.M., Van Steenberg M.E., 1985, ApJ 294, 599
Stickland D.J., 1995, Observatory 115, 180
Trümper J., 1983, Adv. Space Res. 2, No. 4, 241
Walborn N.R., Panek R.J., 1984, ApJ 286, 718
Walter F.M., Kuhi L.V., 1981, ApJ 250, 254
Walter F.M., Kuhi L.V., 1984, ApJ 284, 194
Walter F.M., Brown A., Mathieu R.D., 1988, AJ 96, 297
Wootten A., Sargent A., Knapp G., et al., 1983, ApJ 269, 147
Zimmermann H.U., Belloni T. Izzo C., et al., 1993, MPE report 244

This article was processed by the author using Springer-Verlag LaTeX A&A style file *L-AA* version 3.